

Improved Predictions for Higgs Q_T at the Tevatron and the LHC

Qing-Hong Cao^{1,2}, Chuan-Ren Chen³, Carl Schmidt⁴ and C.-P. Yuan⁴

¹*HEP Divison, Argonne National Laboratory, Argonne, IL 60439, USA*

²*Enrico Fermi Institute, University of Chicago, Chicago, IL 60637, USA*

³*Institute for the Physics and Mathematics of the Universe,
University of Tokyo, Chiba 277-8568, Japan*

⁴*Department of Physics and Astronomy,
Michigan State University, East Lansing, MI 48824, USA*

(Dated: February 6, 2020)

Abstract

The search for the Higgs boson at the Tevatron and the LHC relies on detailed calculations of the kinematics of Higgs boson production and decay. In this paper, we improve the calculation of the distribution in transverse momentum, Q_T , of the Higgs boson in the gluon fusion production process, $gg \rightarrow H$, by matching the resummed distribution at small Q_T with the $\mathcal{O}(\alpha_s^4)$ fixed-order perturbative calculation at high Q_T in the ResBos Monte Carlo program. The distribution is higher at large Q_T than with the old $\mathcal{O}(\alpha_s^3)$ fixed-order perturbative calculation, and the matching with the resummed calculation is much smoother. The total cross section is also increased, more in line with next-to-next-to-leading-order calculations. We also study the effect of the new calculation on the distribution of $\Delta\phi_{\ell\ell}$ in the overall process $gg \rightarrow H \rightarrow W^+W^- \rightarrow \ell^+\ell^-\nu\bar{\nu}$, and the effect of PDF uncertainties on the distributions at the Tevatron and the LHC.

I. INTRODUCTION

It has been over 25 years since the discovery of the W and Z gauge bosons in the UA1 and UA2 colliders at CERN, and we are finally on the verge of discovering the source of their mass. With the on-going studies at the Tevatron collider at Fermilab and the turn-on of the Large Hadron Collider (LHC) at CERN, we will finally be able to probe directly the physics that breaks the electroweak symmetry and distinguishes the massive W and Z bosons from the massless photon. The simplest model of Electroweak Symmetry Breaking (EWSB) is the Standard Model (SM) of particle physics, which contains a complex electroweak scalar doublet that acquires a vacuum expectation value, thereby breaking the electroweak symmetry spontaneously. Three of the degrees of freedom of this complex doublet become the longitudinal modes of the massive W^+ , W^- , and Z bosons, while the remaining degree of freedom is manifested as a single neutral scalar—the SM Higgs boson (H). Although this is not the only possible mechanism for EWSB, the search for the Higgs boson is the benchmark study for EWSB physics to be undertaken at the Tevatron and the LHC. If all goes well, it should be observed or ruled out within the next few years.

The most stringent limits on the Higgs boson mass, m_H , come from direct searches for the particle at LEP2 in the process $e^+e^- \rightarrow ZH$, where the lower bound of 114.1 GeV has been obtained at 95% confidence level (C.L.) [1]. In addition, preliminary results from a combined fit of CDF and DØ data at the Tevatron has been used to exclude the mass range of $160 \text{ GeV} < m_H < 170 \text{ GeV}$ at 95% C.L. [2]. Beyond the direct search for a real Higgs boson, the effect of virtual Higgs bosons in loop calculations can be used to obtain indirect bounds on m_H . Current global fits to electroweak precision measurements, in combination with the direct search limit, prefer $m_H \lesssim 191 \text{ GeV}$ at 95% confidence level [3]. The Tevatron collider has a reasonable chance of discovery or exclusion over much of this preferred range of m_H , assuming 7 fb^{-1} of data obtained by the end of Tevatron running [4]. Furthermore, the LHC can be expected to cover the entire range of Higgs boson masses up to about 1 TeV, which is a rough upper bound on m_H , based on triviality and unitarity of the Standard Model [5].

At both the Tevatron and the LHC the largest channel for production of the Higgs boson is gluon fusion, with the ggH coupling arising via a top quark loop. Other important channels are production of the Higgs boson with an associated W boson, Z boson, or top quark pairs,

as well as production of the Higgs boson through vector-boson or bottom-quark fusion. The importance of each channel for discovery/exclusion of the Higgs boson depends on its mass. A light Higgs boson ($m_H \lesssim 135$ GeV) decays predominantly to bottom quark pairs. In this case the inclusive Higgs boson signal is very difficult to pick out from the very large QCD $b\bar{b}$ background. The best sensitivity at the Tevatron in this mass range is instead found in the WH and ZH associated production channels, where the extra particles can be used to better distinguish the signal from background. A heavier Higgs boson ($m_H \gtrsim 135$ GeV) decays predominantly to W boson pairs with one of the W 's potentially off-shell. In this mass range the inclusive production through gluon fusion is most important at the Tevatron, with the best sensitivity occurring around $m_H \approx 160\text{--}170$ GeV, where the WW decay mode is fully open. These modes and many others were used in the recent combined fit at the Tevatron to exclude the mass range of $160\text{ GeV} < m_H < 170\text{ GeV}$ at 95% C.L. [2] Other important Higgs decay modes, both at the Tevatron and the LHC, are ZZ for high mass Higgs bosons, and tau pairs and photon pairs for low mass Higgs bosons.

In order to best discern the Higgs boson signal from background, it is necessary to have the most accurate predictions possible for the kinematic distributions of the Higgs boson. In the leading order (LO) calculation of the $gg \rightarrow H + X$ cross section, the Higgs boson is produced with exactly zero transverse momentum, $Q_T = 0$. In higher order calculations it can have non-zero Q_T , due to the emission of additional gluons or quarks, but the calculation at any fixed order of perturbation theory diverges as $Q_T \rightarrow 0$. Thus, any fixed-order calculation is unsuitable for the study of the Q_T -dependence of the Higgs boson (except at large Q_T), or for the study of any other kinematic distribution that is strongly affected by soft gluon radiation. Fortunately, the soft-gluon effects that occur for small Q_T can be incorporated into the calculation, either by their direct production in a parton shower Monte Carlo, such as PHYTHIA [6] or HERWIG [7], or by analytic resummation of the associated large logarithms, as proposed by Collins, Soper, and Sterman (CSS) [8, 9, 10]. This systematic resummation in powers of the strong coupling α_s times powers of the large logarithm $\ln(Q/Q_T)$ has been applied to the Higgs boson process, as well as other processes, in the general resummation code ResBos [11]. For the present process, the scale of the resummation, Q , is equal to the invariant mass of the produced Higgs boson, unless otherwise specified.

The resummation of large logarithms at small Q_T has been analyzed for Higgs production

in a number of studies in recent years [12, 13, 14, 15, 16, 17, 18]. The power of the logarithms that are resummed is determined by parameters, which can be extracted order-by-order in α_s from the perturbative Higgs production cross sections. The calculation of the Higgs boson production cross section in gluon-gluon scattering has been calculated at leading order, next-to-leading order (NLO) [19] and next-to-next-to-leading order (NNLO) [20, 21, 22] in the infinite-top-quark-mass limit, and at LO and NLO [23, 24] with full top quark mass dependence. In addition to the QCD corrections, the NLO electroweak (EW) corrections have also been considered in the infinite-top-quark-mass limit [25], and more complete calculations have been performed by including light quark and top quark effects [26, 27]. Recently, the effects of the combined QCD and EW corrections were analyzed [28, 29]. The inclusive differential cross section at non-zero Q_T , which begins at one higher power of α_s , has been calculated at NLO in the infinite-top-mass limit [30, 31, 32], and at LO with full top quark mass dependence [33, 34]. In the infinite-top-quark-mass limit, the heavy top quark loop contracts to an effective gluon-Higgs operator, which simplifies the calculation greatly, effectively reducing the number of loops by one. In addition, it has been shown, at least at NLO, that it is a good approximation to calculate in the infinite top quark mass effective theory, while rescaling by the LO cross section with full top and bottom quark mass dependence [35]. Thus, it has become standard to use this approximation to compute the Higgs boson cross section. For nonzero Q_T this approximation is also good as long as $Q_T \lesssim m_t$ and $m_H \lesssim m_t$ [33, 34].

A recent analysis using the resummation program ResBos to study the phenomenology of Higgs boson production at the Tevatron and the LHC was presented in Ref. [17]. In that work the CSS resummation at small Q_T was matched onto the LO calculation at large Q_T . In this work we have updated the program so that it matches on to the NLO calculation at large Q_T , using the code developed in Ref. [32]. We shall see that this is more consistent with the precision currently included at small Q_T in the resummation program.

The remainder of the paper is organized as follows. In section II we give a brief description of the resummation procedure that is implemented in ResBos. We explain the order of the coefficients used in the resummation calculation and how they are matched on to the fixed-order calculation at large Q_T , and how the improvement is performed to include $\mathcal{O}(\alpha_s^4)$. We also calculate the total production cross sections of the Higgs boson at the Tevatron, the LHC with 10 TeV and 14 TeV center-of-mass (c.m.) energy and compare with NLO

results. In section III we use the updated code of ResBos to produce various kinematic distributions for the Higgs boson. In particular, we emphasize the changes coming from the updated calculation, and note the improvement in the matching between the low and high Q_T regimes. We also discuss the implications of the new predictions on the $\Delta\phi_{\ell\ell}$ correlation of the two charged leptons in the decay $H \rightarrow W^+W^- \rightarrow \ell^+\nu\ell^-\bar{\nu}$. Finally, in section IV we give our conclusions.

II. SOFT GLUON RESUMMATION

A. Formalism

In order to make transparent what we have implemented in the ResBos program, we begin by briefly reviewing the CSS formalism of soft gluon resummation. Resumming the soft gluons and using the narrow width of the Higgs boson to factorize the Higgs production from its subsequent decay, we can write the inclusive differential cross section for $gg \rightarrow H \rightarrow VV \rightarrow 4$ fermions as

$$\begin{aligned} & \frac{d\sigma(gg \rightarrow HX \rightarrow VVX \rightarrow f_1f_2f_3f_4X)}{dQ^2dQ_T^2dyd\phi_Hd\Pi_4} \\ &= \kappa\sigma_0 \frac{Q^2}{2S} \frac{1}{(Q^2 - m_H^2)^2 + (Q^2\Gamma_H/m_H)^2} \left| \mathcal{M}(H \rightarrow VV \rightarrow f_1f_2f_3f_4) \right|^2 \\ &\times \left\{ \frac{1}{(2\pi)^2} \int d^2b e^{iQ_T \cdot b} \tilde{W}_{gg}(b_*, Q, x_1, x_2, C_{1,2,3}) \tilde{W}_{gg}^{NP}(b, Q, x_1, x_2) + Y(Q_T, Q, x_1, x_2, C_4) \right\}, \end{aligned} \quad (1)$$

where S is the square of the center-of-mass energy; V and f_i denote vector boson and fermion, respectively; Q , Q_T , y , ϕ_H and Γ_H are the invariant mass, transverse momentum, rapidity, azimuthal angle and total decay width of the Higgs boson, respectively, defined in the lab frame; and $d\Pi_4$ represents the four-body phase space of the Higgs boson decay, defined in the Collin-Soper frame [36]. In Eq. (1), the quantity

$$\sigma_0 = \frac{\sqrt{2} G_F \alpha_s^2}{576 \pi}, \quad (2)$$

arises as an overall factor in the infinite-top-quark-mass limit. We have multiplied this by an additional factor

$$\kappa = \frac{\sigma^{\text{LO}}(m_t, m_b, m_c)}{\sigma^{\text{LO}}(\infty, 0, 0)}, \quad (3)$$

which takes into account the masses of the top, bottom, and charm quarks at LO. It has been shown that multiplying the NLO Higgs cross section in the infinite-top-quark-mass limit by the factor κ is a good approximation to the full mass-dependent NLO cross section over a wide range of Higgs boson masses [35]. In Eq. (1), $|\mathcal{M}(\cdots)|^2$ denotes the matrix element squared of the Higgs boson decay whose analytical expressions are given in Ref. [17].

In Eq. (1), the term containing \tilde{W}_{gg} dominates at small Q_T , growing as Q_T^{-2} times a resummation in powers of $\ln Q^2/Q_T^2$, to all orders in α_s . It can be expressed as

$$\tilde{W}_{gg}(b, Q, x_1, x_2, C_{1,2,3}) = e^{-S(b, Q, C_1, C_2)} \sum_{a,b} (C_{ga} \otimes f_a)(x_1) (C_{gb} \otimes f_b)(x_2), \quad (4)$$

where the Sudakov exponent is given by

$$S(b, Q, C_1, C_2) = \int_{C_1^2/b^2}^{C_2^2 Q^2} \frac{d\bar{\mu}}{\bar{\mu}^2} \left[A(\alpha_s(\bar{\mu}), C_1) \ln \left(\frac{C_2^2 Q^2}{\bar{\mu}^2} \right) + B(\alpha_s(\bar{\mu}), C_1, C_2) \right]. \quad (5)$$

$$(6)$$

The coefficients A and B and the functions C_{ga} can be expanded as a power series in α_s :

$$A(\alpha_s(\bar{\mu}), C_1) = \sum_{n=1}^{\infty} \left(\frac{\alpha_s(\bar{\mu})}{\pi} \right)^n A^{(n)}(C_1), \quad (7)$$

$$B(\alpha_s(\bar{\mu}), C_1, C_2) = \sum_{n=1}^{\infty} \left(\frac{\alpha_s(\bar{\mu})}{\pi} \right)^n B^{(n)}(C_1, C_2), \quad (8)$$

and

$$C_{ga}(x, b, \mu, C_1, C_2) = \sum_{n=0}^{\infty} \left(\frac{\alpha_s(\mu)}{\pi} \right)^n C_{ga}^{(n)}(z, b, \mu, \frac{C_1}{C_2}), \quad (9)$$

with $\mu = C_3/b$. These quantities can be extracted order-by-order from the fixed-order calculations. In our numerical results, we have included $A^{(1,2,3)}$, $B^{(1,2)}$ and $C^{(0,1)}$, whose analytical expressions are given in Appendix A for completeness. We use the canonical choice for the renormalization constants, $C_1 = C_3 = 2e^{-\gamma_E}$, $C_2 = C_4 = 1$, which simplifies the above expressions. The function \tilde{W}_{gg}^{NP} describes the non-perturbative part of the soft-gluon resummation, in which we use the BLNY parameterization [37].

Finally, in Eq. (1), the term containing Y incorporates the remainder of the cross section, which is less singular as $Q_T \rightarrow 0$ than the \tilde{W}_{gg} -term. It consists of the difference between the full cross section at finite Q_T and the small- Q_T limit of this cross section, each calculated to the same order in α_s . At small Q_T , these cancel, so that the contribution of the Y -term

is small, and the resummed term dominates. At large Q_T , where the logarithms become small, the resummed term cancels against the small- Q_T limit term (to the given order in α_s), so that the cross section approaches the fixed-order calculation. More details of how this matching process between the resummed calculation and the fixed-order calculation is implemented in ResBos can be found in Ref. [11]. In previous studies of Higgs boson production at hadron colliders [12, 17], the high Q_T perturbative calculation was included in ResBos at $\mathcal{O}(\alpha_s^3)$. The major update to the program that we have incorporated in this paper is to include the high Q_T perturbative calculation at $\mathcal{O}(\alpha_s^4)$. This was done by using the code of Ref. [32] to rescale the perturbative piece of the grids used by the ResBos code by the factor $(\text{Pert}(\alpha_s^3) + \text{Pert}(\alpha_s^4)) / \text{Pert}(\alpha_s^3)$, where $\text{Pert}(\alpha_s^3)$ and $\text{Pert}(\alpha_s^4)$ are the contributions to the Q_T distribution of the Higgs boson of order α_s^3 and α_s^4 , respectively.

Note that the description of the perturbative piece in terms of LO, NLO, or NNLO is problematic; for example, $\mathcal{O}(\alpha_s^4)$ would be considered as NLO when referring to the (non-zero) transverse momentum distribution, but it would be considered as NNLO when referring to the total Higgs production cross section. Thus, we will refer to the power of α_s when comparing the precision of the perturbative piece of the calculation used in this work ($\mathcal{O}(\alpha_s^4)$) versus that used in the previous works ($\mathcal{O}(\alpha_s^3)$).

B. Predictions of the total cross section for $gg \rightarrow HX$ at hadron colliders

The primary use of the resummation code ResBos is for the calculation of the transverse momentum spectrum, as well as other distributions that are influenced strongly by soft gluon effects. However, it also gives a calculation of the total cross section that is comparable to that of a fixed-order calculation, depending on the order to which the resummation coefficients have been included. We have included all of the coefficients ($A^{(1,2)}$, $B^{(1)}$, $C^{(0,1)}$) in ResBos that are necessary to produce a NLO calculation of the cross section. In addition, we also have included the NNLO coefficients $A^{(3)}$ and $B^{(2)}$ and are only missing the function $C^{(2)}$ that is necessary to give a NNLO calculation of the total cross section. The function $C^{(2)}$ should be extractable from the NNLO analytic expression of the cross section, but this has not been achieved as yet. Thus, our calculation of the cross section should be comparable to a NLO fixed-order calculation, and in fact contains much of the (presumably dominant) contributions at NNLO.

	LHC 14 TeV			LHC 10 TeV			Tevatron 1.96 TeV		
m_H (GeV)	RES	NLO ^{RES}	NLO ^{Higlu}	RES	NLO ^{RES}	NLO ^{Higlu}	RES	NLO ^{RES}	NLO ^{Higlu}
140	32.12	25.79	27.23	18.09	14.37	15.16	0.50	0.37	0.39
150	28.85	22.97	24.09	15.85	12.67	13.28	0.40	0.30	0.32
160	25.61	20.61	21.50	14.05	11.25	11.74	0.33	0.24	0.26
170	23.03	18.60	19.31	12.54	10.06	10.45	0.27	0.20	0.21

TABLE I: Production cross section of the SM Higgs boson via the gluon fusion process, $gg \rightarrow HX$, in pb at the LHC and Tevatron. We show the results for both 14 TeV and 10 TeV c.m. energy at the LHC and 1.96 TeV c.m. energy at the Tevatron. The label RES indicates the results of resummation calculations predicted from ResBos, and the labels NLO^{RES} and NLO^{Higlu} indicate the NLO results calculated from ResBos and Higlu codes, respectively.

In the remainder of this section we compare the predictions for the total cross section from ResBos against NLO predictions. In table I, we present the total cross sections of $gg \rightarrow HX$ for several benchmark points from the resummation (RES) calculations using the updated ResBos program with CTEQ6.6M PDF [38]. These are compared to an expansion of the resummation formula to NLO (RES-NLO), and also to an exact NLO calculation. The former is an exact NLO QCD calculation with the same implementation for including the effect of the masses of the top, bottom, and charm quarks at LO, cf. Eq. (3). The latter is calculated with the help of the public code HIGLU [39].^{#1} We note that the main difference between these two NLO calculations is in the handling of the quark mass dependences. As explained in section II A, the resummed calculation, as well as the RES-NLO calculation, is performed in the heavy top quark mass limit, with the quark mass dependence included by the LO factor κ given in Eq. 3. On the contrary, HIGLU uses the exact NLO two-loop calculation, including both the top quark and the bottom quark in the loop.

The cross section is consistently higher in the resummed calculation (RES) than for the NLO calculations, due to the enhancement from the NNLO corrections. This is seen more easily in Fig. 1, which displays the cross section of the Higgs boson production as a function of m_H at the LHC and Tevatron, where the black, blue and red curves denote the RES,

^{#1} More detailed analysis of the HIGLU calculation, e.g. the PDF uncertainties and scale dependence, are given in the Appendix B.

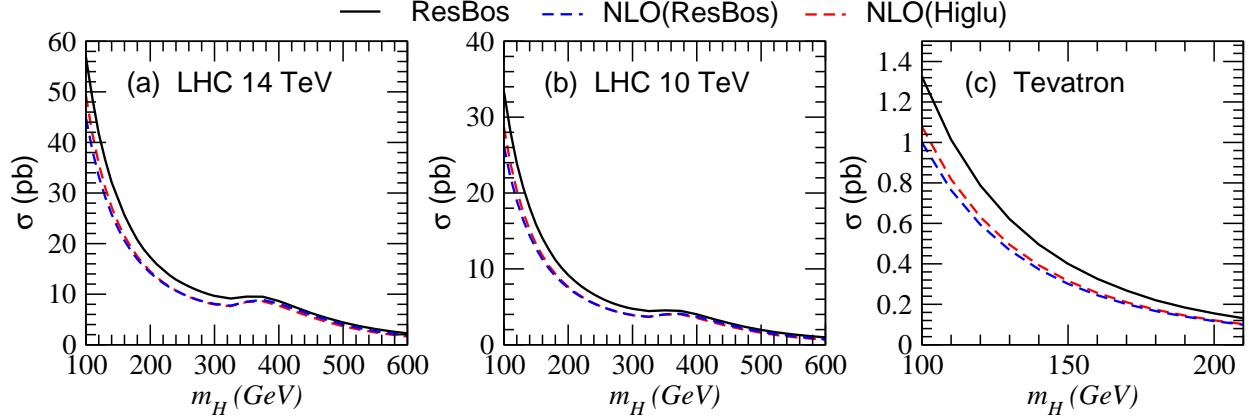


FIG. 1: The resummation the total cross section for $gg \rightarrow HX$ at the LHC and the Tevatron using the updated ResBos program with CTEQ6.6M PDF. We consider both 10 TeV and 14 TeV c.m. energy at the LHC and 1.96 TeV c.m. energy at Tevatron. The NLO predictions from ResBos and Higlu programs are also shown.

RES-NLO and HIGLU results, respectively. We display explicitly the enhancement in the cross section in the resummed calculation in Fig. 2, where we plot the ratio of the RES cross section to the NLO cross section, both for the RES-NLO and the HIGLU calculations. The ratio of RES to NLO drops rapidly when $m_H \gtrsim 300$ GeV and reaches a minimum for $m_H \sim 380$ GeV. This unusual dependence on m_H can be traced to the handling of the virtuality of the Higgs boson in the calculations. The HIGLU calculation is for an explicitly on-shell Higgs boson production without the subsequent Higgs boson decay, i.e. $\delta(Q^2 - m_H^2)$. The same is also true for the RES-NLO calculation. On the contrary, the ResBos code takes into account the Breit-Wagner width effects, see Eq. (1), to perform a realistic simulation. Thus, the cross section is calculated for an off-shell Higgs boson of mass-squared Q^2 , which is then convoluted with the Breit-Wigner. This gives a sizable effect when the Higgs width is large, and in particular for masses around 300-400 GeV ($m_H \gtrsim 2m_t$) where the cross section curves have noticeable structure.

III. NUMERICAL STUDY OF $gg \rightarrow H \rightarrow WW^{(*)} \rightarrow \ell\ell\nu\nu$

For our analysis of kinematic distributions, we will use several benchmark values for the Higgs boson mass: $m_H = 140, 150, 160$ and 170 GeV at the Tevatron RUN II, and $m_H = 160$ GeV at the LHC. We will focus on the most promising discovery mode for this mass range,

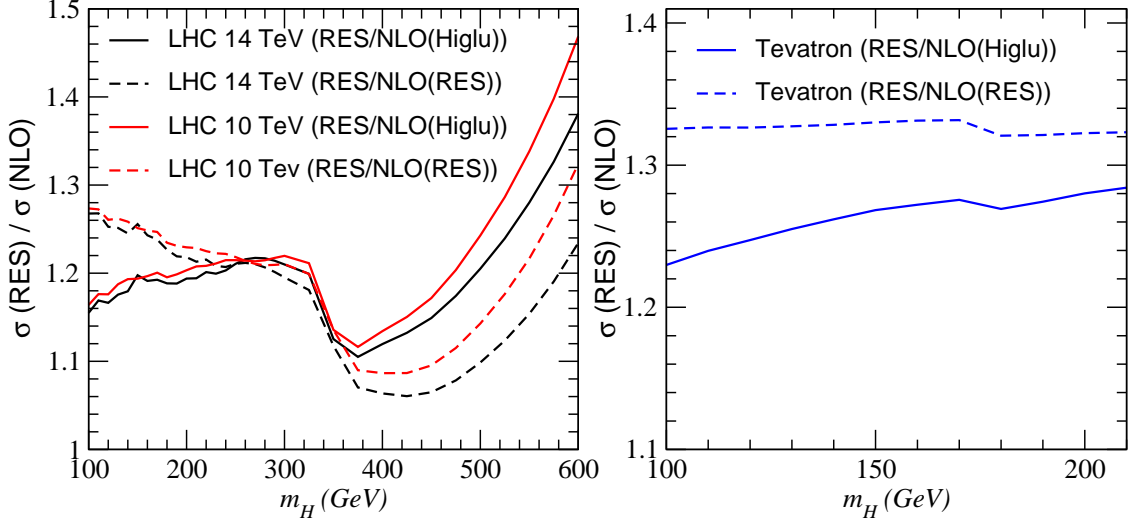


FIG. 2: The ratio of the total cross section of $gg \rightarrow HX$ predicted from the resummation calculation to that from NLO calculations at the LHC and the Tevatron.

which is $gg \rightarrow H \rightarrow W^+W^- \rightarrow \ell^+\ell^-\nu\bar{\nu}$, where ℓ^\pm denotes a charged lepton and $\nu(\bar{\nu})$ is a neutrino (anti-neutrino). Note that all of the cross sections given in this section include the decay branching ratio of the Higgs boson and that the flavors of leptons are not summed over.

We begin with the transverse momentum distribution of the Higgs boson at the Tevatron, displayed in Fig. 3. The cyan lines and the black dash lines are the predictions with matching at high Q_T to $\mathcal{O}(\alpha_s^4)$ and $\mathcal{O}(\alpha_s^3)$ fixed-order perturbative calculations, respectively, and the bands show the PDF uncertainties. The peak position (at $Q_T \sim 10$ GeV) is the same for both the dash and cyan lines, since this is determined exclusively by the resummed contribution to the calculation. At high Q_T , however, the distribution is determined mainly by the perturbative contribution, and it is substantially higher for the $\mathcal{O}(\alpha_s^4)$ calculation. We also note that the $\mathcal{O}(\alpha_s^4)$ perturbative contribution matches much more smoothly with the resummed contribution. This is particularly apparent when plotted with a logarithmic scale, as in the lower panel of Fig. 3, where the unphysical kink around $Q_T \sim 70$ GeV in the $\mathcal{O}(\alpha_s^3)$ curve is absent in the $\mathcal{O}(\alpha_s^4)$ curve. Similarly, we show the improved Q_T distribution of the Higgs boson at the LHC in Fig. 4, including PDF uncertainties as well. The kink seen in the $\mathcal{O}(\alpha_s^3)$ dashed line is shifted to higher Q_T (~ 110 GeV) compared with the case at the Tevatron. With matching to the $\mathcal{O}(\alpha_s^4)$ calculation, the curve becomes much more smooth. The uncertainty at the peak region is about 8% and increases to higher than 10%

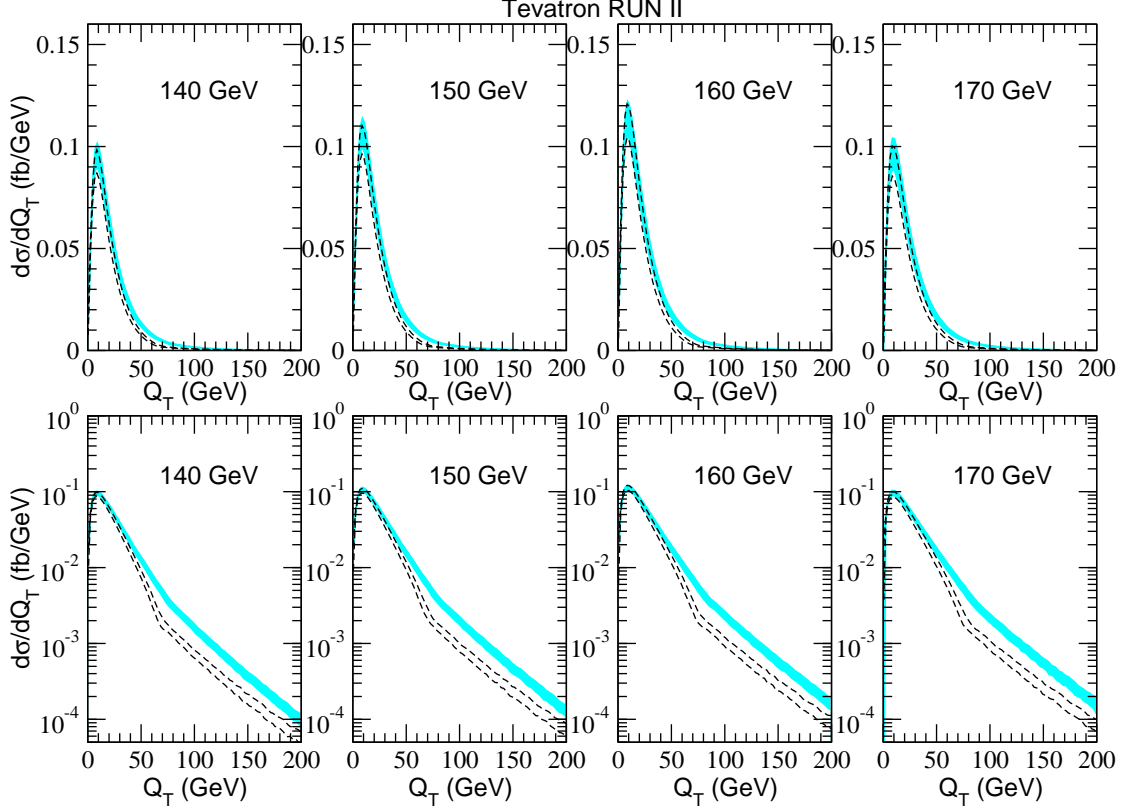


FIG. 3: Transverse momentum, Q_T , of the SM Higgs boson at the Tevatron. The plots in the lower panel are the same as those in the upper panel, except for using a logarithmic scale for the y-axis. The dashed lines and cyan lines are the calculations when matching at high Q_T to the $\mathcal{O}(\alpha_s^3)$ and $\mathcal{O}(\alpha_s^4)$ fixed-order perturbative contributions, respectively, and the bands reflect the PDF uncertainties..

when Q_T is larger than 40 GeV for all curves at the Tevatron, while the uncertainty stays at about 2% \sim 6% for the full range of Q_T at the LHC.

We can use the updated Q_T distributions at the LHC and the Tevatron to study the dependence of this distribution on the collider c.m. energy. The peak position, $Q_T(\text{peak})$, only changes mildly with the c.m. energy. For example, $Q_T(\text{peak})$ is roughly 10 GeV, 13 GeV and 13 GeV at the Tevatron, LHC 10 TeV and LHC 14 TeV c.m. energy, respectively, for $m_H = 160$ GeV. On the other hand, the average transverse momentum, $\langle Q_T \rangle$, increases more substantially when the mass of the Higgs boson or the energy of the collider increases. For $m_H = 160$ GeV and taking the average in the region of $0 \leq Q_T \leq 200$ GeV, we find that $\langle Q_T \rangle$ increases from about 26 GeV at the Tevatron to about 40 GeV and 43 GeV at

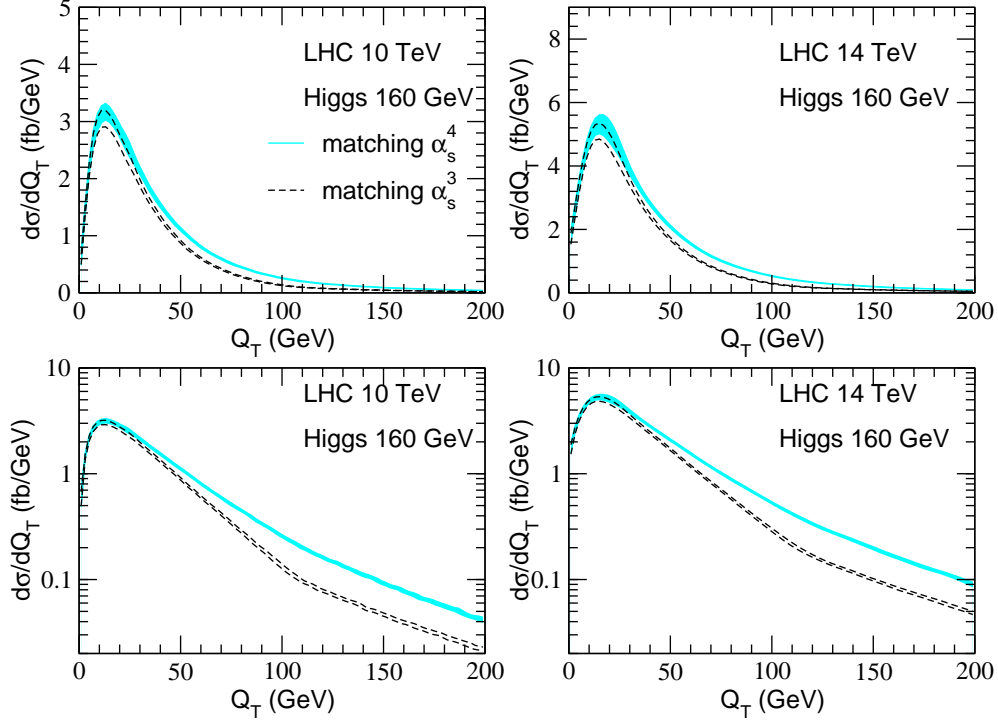


FIG. 4: The same as Fig. 3, but for the SM Higgs boson at the LHC.

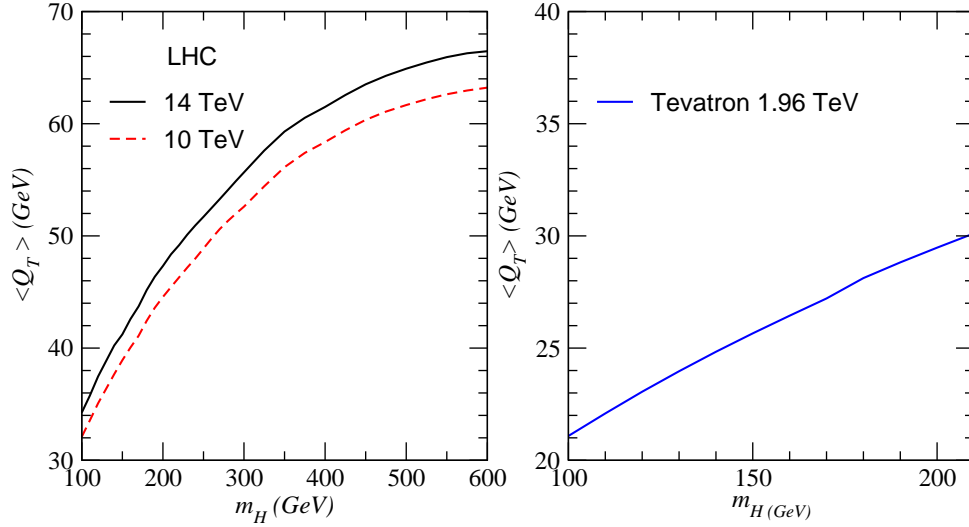


FIG. 5: The average of Q_T (in the region of $0 \leq Q_T \leq 200$ GeV) of the Higgs boson at the LHC and the Tevatron.

the LHC with 10 TeV and 14 TeV c.m. energy, respectively. The dependence of $\langle Q_T \rangle$ on the Higgs boson mass at the various colliders is shown in Fig. 5.

Finally, we consider the distribution in the difference in azimuthal angle of the two charged

leptons in the Higgs boson decay, $\Delta\phi_{\ell\ell}$, which is useful for making cuts to extract the Higgs boson signal from background. This distribution is shown for the Tevatron in Fig. 6. The solid and dash lines in the lower panel are the calculations when matching to $\mathcal{O}(\alpha_s^4)$ and $\mathcal{O}(\alpha_s^3)$ at high Q_T , respectively. From these plots we see that the signal process $gg \rightarrow H \rightarrow W^+W^- \rightarrow \ell^+\ell^-\nu\bar{\nu}$ prefers to have the charged leptons both moving in the same direction near $\Delta\phi_{\ell\ell} \approx 0$. This can be understood from angular momentum conservation and the left-handed nature of the W -boson decays. In the Higgs boson rest frame, the W^+ and W^- are produced back-to-back with opposite spins. The W^- boson decays with the charged lepton momentum anti-correlated with the W^- spin, while the W^+ boson decays with the charged anti-lepton momentum correlated with the W^+ spin. As a result the two charged leptons tend to move in the same direction. This feature still holds even when only one of the W bosons from the Higgs boson decay is on-shell. On the other hand, the background events, which predominantly originate from W^+W^- pair production, are more likely to be produced with the charged leptons back-to-back with $\Delta\phi_{\ell\ell} \approx \pi$.

The enhancement of the distribution due to the improved calculation is exhibited in the plots in the upper panel of Fig. 6, where the blue line is the ratio of the solid curve to the dash curve. From these figures we see that the new calculation with matching at $\mathcal{O}(\alpha_s^4)$ enhances $\Delta\phi_{\ell\ell}$ by about from 14% to 18% over the old calculation. Interestingly, the largest enhancement occurs at $\Delta\phi_{\ell\ell} \approx 0$, while the enhancement has a minimum around $\Delta\phi_{\ell\ell} \approx 2$ radians. Similarly, in the $\Delta\phi_{\ell\ell}$ distribution at the LHC, which is shown in Fig. 7, the enhancement due to the improved matching varies between 16% \sim 23%, which is slightly larger than for the Tevatron. The change in the shape of the $\Delta\phi_{\ell\ell}$ distribution between the $\mathcal{O}(\alpha_s^3)$ and the $\mathcal{O}(\alpha_s^4)$ calculations can be considered purely kinematical, since the Higgs boson is spinless, and the comparable distribution in the Higgs boson rest frame would not be affected by changes in the production cross section. In the lab frame, however, the distribution is affected by the fact that the cross section is larger at high Higgs boson Q_T in the $\mathcal{O}(\alpha_s^4)$ calculation, so that more of the charged lepton pairs are produced with a bigger momentum boost.

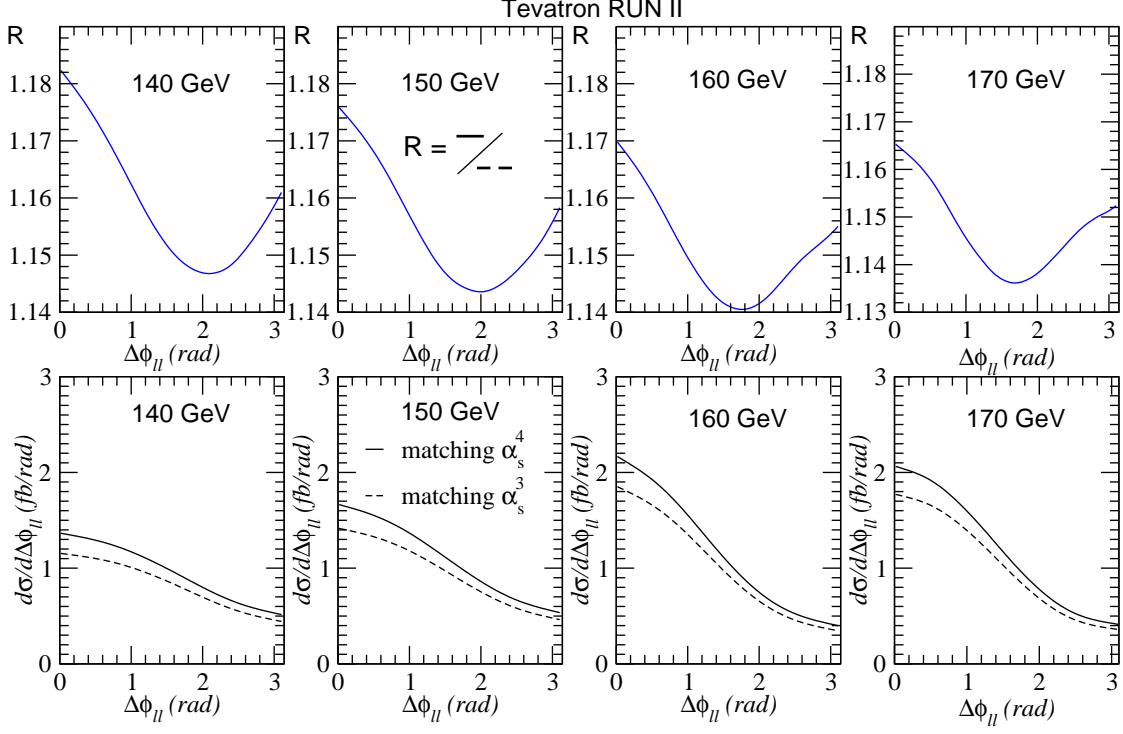


FIG. 6: $\Delta\phi_{\ell\ell}$ distributions at the Tevatron. The solid and the dash curves in the lower panel are the calculations when matching at high Q_T to the $\mathcal{O}(\alpha_s^3)$ and $\mathcal{O}(\alpha_s^4)$ fixed-order calculations, respectively.

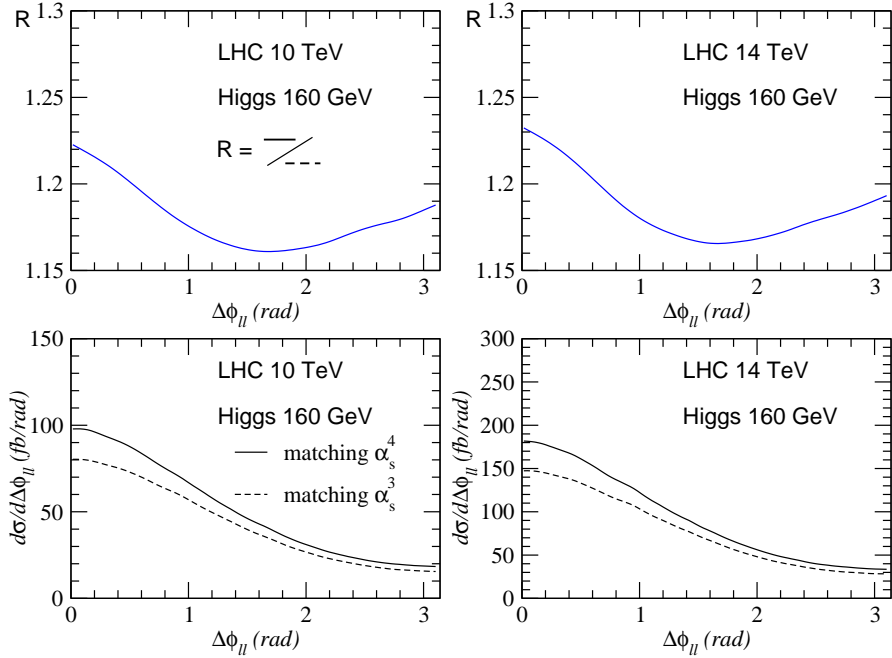


FIG. 7: The same as Fig. 6 but for the LHC.

IV. CONCLUSION

The search for the Higgs boson at the Tevatron and the LHC relies on detailed knowledge of the distributions (event rate and shape) of the Higgs decay products. These, in turn, are sensitive to the kinematics of the Higgs boson production. In this paper, we improve the calculation of the transverse momentum, Q_T , distribution of the Higgs boson in the gluon fusion production process, $gg \rightarrow H$, at the Tevatron and the LHC by matching the resummed distribution at small Q_T with the $\mathcal{O}(\alpha_s^4)$ fixed-order perturbative calculation at high Q_T in the ResBos Monte Carlo program. The total cross section of $gg \rightarrow HX$ predicted from the updated ResBos is always larger than NLO calculation and the enhancement can reach about 40% at the LHC for a heavy Higgs boson. The difference between RES and NLO calculation becomes minimum ($\sim 10\%$) in the threshold regime of $m_H \gtrsim 2m_t$. The unphysical kink, which had been obtained when matching at high Q_T with the $\mathcal{O}(\alpha_s^3)$ fixed-order perturbative calculation, is removed. The PDF uncertainties are studied in the Q_T distributions as well. At the Tevatron we find the uncertainty to be about 5% in the peak area and larger than 10% in the region of $Q_T \gtrsim 50$ GeV. At the LHC, the uncertainty is about 2% \sim 6% for the entire region of Q_T . For the comparison of Q_T , we found that the average value of Q_T increases when the c.m. energy or the mass of the Higgs boson increases, however, peak position is insensitive to both. We finally study the opening azimuthal angle, $\Delta\phi_{\ell\ell}$, of the two charged leptons in the Higgs boson decay, $H \rightarrow W^+W^- \rightarrow \ell^+\ell^-\nu\bar{\nu}$. The distribution of $\Delta\phi_{\ell\ell}$ is enhanced by 14% \sim 18% and 16% \sim 23% at the Tevatron and the LHC, respectively, with the largest enhancement occurring at small opening angles. With current and expected integrated luminosity, the Tevatron has the capability to discover or exclude the SM Higgs boson over a significant range of mass. Detailed predictions of the kinematics of the Higgs boson, such as its transverse momentum distribution, play a crucial role in this analysis. This is our motivation for the continued improvement of the ResBos program and for this study.

Acknowledgments

Q.H.C. is supported in part by the Argonne National Laboratory and University of Chicago Joint Theory Institute (JTI) Grant 03921-07-137, and by the U.S. Department

of Energy under Grants No. DE-AC02-06CH11357 and No. DE-FG02-90ER40560. C.R.C is supported by World Premier International Research Center Initiative (WPI Initiative), MEXT, Japan. C.S. and C.P.Y. acknowledge the support of the U.S. National Science Foundation under grant PHY-0555544 and PHY-0555545. C.P.Y. would also like to thank the hospitality of National Center for Theoretical Sciences in Taiwan and Center for High Energy Physics, Peking University, in China, where part of this work was done.

APPENDIX A: A, B, AND C COEFFICIENTS

For completeness, we give expressions for the so-called A , B , and C coefficients used in our resummation calculations. In our numerical result, we have used $A^{(1,2)}$, $B^{(1)}$ [40], $B^{(2)}$ [41, 42], $A^{(3)}$ [43] and $C^{(0,1)}$ [44, 45]. Their analytical expressions for the process $gg \rightarrow H$ are much simplified in the canonical choice of the renormalization constants, $C_1 = C_3 = 2e^{-\gamma_E}$, $C_2 = C_4 = 1$, which we use in this project. For this choice of renormalization constants, we have:

$$A_g^{(1)} = C_A, \tag{A1}$$

$$A_g^{(2)} = C_A \left[\left(\frac{67}{36} - \frac{\pi^2}{12} \right) N_c - \frac{5}{18} N_f \right], \tag{A2}$$

$$\begin{aligned} A_g^{(3)} = & \frac{C_A C_F N_f}{2} \left(\zeta(3) - \frac{55}{48} \right) - \frac{C_A N_f^2}{108} + C_A^3 \left(\frac{11\zeta(3)}{24} + \frac{11\pi^4}{720} - \frac{67\pi^2}{216} + \frac{245}{96} \right) \\ & + C_A^2 N_f \left(-\frac{7\zeta(3)}{12} + \frac{5\pi^2}{108} - \frac{209}{432} \right), \end{aligned} \tag{A3}$$

where $C_A = 3$, $N_c = 3$, $N_f = 5$, $C_F = 4/3$ and the Riemann constant $\zeta(3) = 1.202\dots$;

$$B_g^{(1)} = -\beta_0, \tag{A4}$$

$$B_g^{(2)} = -\frac{1}{2} \left[C_A^2 \left(\frac{8}{3} + 3\zeta(3) \right) - C_F T_R N_f - \frac{4}{3} C_A T_R N_f \right] + \beta_0 \left[\frac{C_A \pi^2}{12} + \frac{11 + 3\pi^2}{4} \right], \tag{A5}$$

where $\beta_0 = (11N_c - 2N_f)/6$ and $T_R = 1/2$;

$$C_{gg}^{(0)}(x) = \delta(1-x), \quad (\text{A6})$$

$$C_{gq}^{(0)}(x) = 0, \quad (\text{A7})$$

$$C_{gg}^{(1)}(x) = \delta(1-x) \frac{11 + 3\pi^2}{4}, \quad (\text{A8})$$

$$C_{gq}^{(1)}(x) = \frac{C_F}{2}x, \quad (\text{A9})$$

where x is the momentum fraction carried by the gluon after splitting from its mother particle (gluon g or quark q).

APPENDIX B: TOTAL CROSS SECTIONS OF $gg \rightarrow HX$ AT NLO

In this section we evaluate the uncertainties in the cross section due to uncertainties in the PDFs and due to higher order corrections, as illuminated by renormalization scale dependence. Since we have used the code HIGLU [39] as a reference comparison for the total cross section in our resummation calculation (see for example Fig. 1), we will use it to produce numerical results in this section. We expect the uncertainties in the total cross section in the resummed calculation to be comparable. Note that the Higgs boson decay is not implemented in HIGLU, so all the results presented in this appendix are for on-shell Higgs boson production only.

In Fig. 8, we display the uncertainties both due to the PDF uncertainties and due to the scale dependence. The uncertainties due to the PDFs (primarily the gluon PDF), relative to the cross section with the best-fit PDF, is shown by the bands in Fig. 8. The PDF error is calculated from the master formula given in Eq. (2.5) in Ref. [46], using the 44 sets of CTEQ6.6M package. For $100 \text{ GeV} \leq m_H \leq 600 \text{ GeV}$, the uncertainty is smaller than 5% at the LHC with a c.m. energy of both 14 TeV and 10 TeV. In the intermediate mass region, $200 \text{ GeV} \lesssim m_H \lesssim 300 \text{ GeV}$, where the gluon PDF is more constrained, the uncertainty is reduced to about 2% \sim 3%. Setting $x_1 \approx x_2 = x$ where $x_{1,2}$ is the momentum fraction of the incoming parton, and using $\hat{s} = x_1 x_2 s$, we obtain $\langle x \rangle \approx m_H / \sqrt{s}$. From this we see that the minimum in the PDF uncertainty in both Fig. 8(a) and (b) occurs around $\langle x \rangle \sim 0.022$. On the contrary, the Higgs boson production cross section at the Tevatron suffers from much larger PDF uncertainties. For example, the uncertainty increases from 5% to 14% for the mass of Higgs boson mass $100 \text{ GeV} \leq m_H \leq 200 \text{ GeV}$.

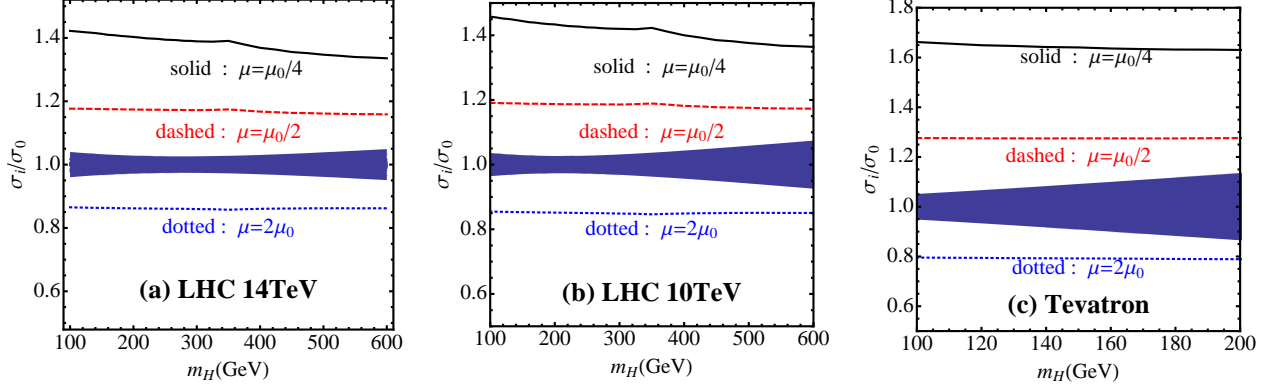


FIG. 8: The PDF uncertainties of the NLO total cross section of $gg \rightarrow HX$ shown in bands and the dependence on the renormalization scale at the LHC and Tevatron using the CTEQ6.6M PDFs. The renormalization and factorization scales $\mu = \mu_R = \mu_F$ are set to $\mu_0/4$, $\mu_0/2$ and $2\mu_0$, where $\mu_0 = m_H$, and the ratio is taken with respect to the cross section evaluated with $\mu = \mu_0$.

We also display the uncertainties in the cross section calculation at NLO due to the renormalization scale (μ_R) and factorization scale (μ_F) dependence in Fig. 8. These uncertainties can be considered as an estimate of the size of the unknown higher order corrections. For this study, we have set $\mu = \mu_R = \mu_F$ and vary it around the central value of $\mu_0 = m_H$. Typically, a factor of 2 is used to estimate the size of the higher order corrections, so we have displayed curves with $\mu = 2\mu_0$ and $\mu = \mu_0/2$. In addition, since the NNLO QCD corrections prefer a scale of $\mu = \mu_0/4$ [21], we also display a curve with that value. In Fig. 8 we plot the ratio $\sigma(\mu_i)/\sigma(\mu_0)$ as a function of m_H both at the LHC and at the Tevatron. The cross sections vary between about -15% for $\mu = 2\mu_0$ and $+20\%$ for $\mu = \mu_0/2$ at the LHC, and can reach about $+40\%$ when using $\mu = \mu_0/4$. At the Tevatron, the scale dependences are even larger. We note that the scale dependence at both colliders is insensitive to m_H and dominates over the PDF uncertainties.

The PDF uncertainties can be improved further by using the new set of CTEQ PDFs (named CT09 [47]), which take into account the recent inclusive jet data at the Tevatron [48, 49]. Fig. 9 shows the relative error, $\delta\sigma$, in the Higgs boson production cross section due to PDF uncertainties derived from CT09 (black) and CTEQ6.6M (red). The uncertainties in the Higgs boson production cross section are improved substantially using the new set of PDFs, both at the LHC and at the Tevatron. Due to the modification of the gluon PDF,

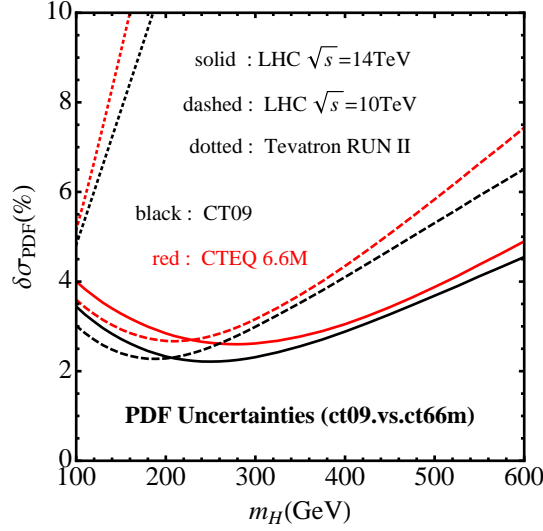


FIG. 9: The uncertainties of the NLO total cross section of $gg \rightarrow HX$ due to the PDFs. The red curves are for CTEQ6.6M and the black curves are for CT09.

the minima of the PDF uncertainties at the LHC are shifted to smaller values of the Higgs boson mass.

-
- [1] LEP Working Group for Higgs boson searches, R. Barate *et al.*, Phys. Lett. **B565**, 61 (2003), arXiv:hep-ex/0306033.
 - [2] Tevatron New Phenomena and Higgs working group, for the CDF and DZero collaborations, (2009), arXiv:arXiv:0903.4001[hep-ex].
 - [3] The LEP Electroweak Working Group.
 - [4] A. Duperrin, (2008), arXiv:arXiv:0805.3624 [hep-ex].
 - [5] C. F. Kolda and H. Murayama, JHEP **07**, 035 (2000), arXiv:hep-ph/0003170.
 - [6] T. Sjostrand, S. Mrenna, and P. Skands, Comput. Phys. Commun. **178**, 852 (2008), arXiv:arXiv:0710.3820 [hep-ph].
 - [7] G. Corcella *et al.*, (2002), arXiv:hep-ph/0210213.
 - [8] J. C. Collins and D. E. Soper, Nucl. Phys. **B193**, 381 (1981).
 - [9] J. C. Collins and D. E. Soper, Nucl. Phys. **B197**, 446 (1982).
 - [10] J. C. Collins, D. E. Soper, and G. Sterman, Nucl. Phys. **B250**, 199 (1985).
 - [11] C. Balazs and C.-P. Yuan, Phys. Rev. **D56**, 5558 (1997), hep-ph/9704258.

- [12] C. Balazs and C. P. Yuan, Phys. Lett. **B478**, 192 (2000), arXiv:hep-ph/0001103.
- [13] E. L. Berger and J.-W. Qiu, Phys. Rev. **D67**, 034026 (2003), arXiv:hep-ph/0210135.
- [14] A. Kulesza, G. Sterman, and W. Vogelsang, Phys. Rev. **D69**, 014012 (2004), arXiv:hep-ph/0309264.
- [15] G. Bozzi, S. Catani, D. de Florian, and M. Grazzini, Phys. Lett. **B564**, 65 (2003), arXiv:hep-ph/0302104.
- [16] G. Bozzi, S. Catani, D. de Florian, and M. Grazzini, Nucl. Phys. **B737**, 73 (2006), arXiv:hep-ph/0508068.
- [17] Q.-H. Cao and C.-R. Chen, Phys. Rev. **D76**, 073006 (2007), arXiv:arXiv:0704.1344 [hep-ph].
- [18] G. Bozzi, S. Catani, D. de Florian, and M. Grazzini, Nucl. Phys. **B791**, 1 (2008), arXiv:0705.3887.
- [19] S. Dawson, Nucl. Phys. **B359**, 283 (1991).
- [20] R. V. Harlander and W. B. Kilgore, Phys. Rev. Lett. **88**, 201801 (2002), arXiv:hep-ph/0201206.
- [21] C. Anastasiou and K. Melnikov, Nucl. Phys. **B646**, 220 (2002), arXiv:hep-ph/0207004.
- [22] V. Ravindran, J. Smith, and W. L. van Neerven, Nucl. Phys. **B665**, 325 (2003), arXiv:hep-ph/0302135.
- [23] A. Djouadi, M. Spira, and P. M. Zerwas, Phys. Lett. **B264**, 440 (1991).
- [24] D. Graudenz, M. Spira, and P. M. Zerwas, Phys. Rev. Lett. **70**, 1372 (1993).
- [25] A. Djouadi and P. Gambino, Phys. Rev. Lett. **73**, 2528 (1994), arXiv:hep-ph/9406432.
- [26] U. Aglietti, R. Bonciani, G. Degrassi, and A. Vicini, Phys. Lett. **B595**, 432 (2004), arXiv:hep-ph/0404071.
- [27] G. Degrassi and F. Maltoni, Phys. Lett. **B600**, 255 (2004), arXiv:hep-ph/0407249.
- [28] S. Actis, G. Passarino, C. Sturm, and S. Uccirati, Phys. Lett. **B670**, 12 (2008), arXiv:0809.1301.
- [29] C. Anastasiou, R. Boughezal, and F. Petriello, JHEP **04**, 003 (2009), arXiv:0811.3458.
- [30] D. de Florian, M. Grazzini, and Z. Kunszt, Phys. Rev. Lett. **82**, 5209 (1999), arXiv:hep-ph/9902483.
- [31] V. Ravindran, J. Smith, and W. L. Van Neerven, Nucl. Phys. **B634**, 247 (2002), arXiv:hep-ph/0201114.
- [32] C. J. Glosser and C. R. Schmidt, JHEP **12**, 016 (2002), arXiv:hep-ph/0209248.

- [33] R. K. Ellis, I. Hinchliffe, M. Soldate, and J. J. van der Bij, Nucl. Phys. **B297**, 221 (1988).
- [34] U. Baur and E. W. N. Glover, Nucl. Phys. **B339**, 38 (1990).
- [35] M. Kramer, E. Laenen, and M. Spira, Nucl. Phys. **B511**, 523 (1998), arXiv:hep-ph/9611272.
- [36] J. C. Collins and D. E. Soper, Phys. Rev. **D16**, 2219 (1977).
- [37] F. Landry, R. Brock, P. M. Nadolsky, and C. P. Yuan, Phys. Rev. **D67**, 073016 (2003), arXiv:hep-ph/0212159.
- [38] P. M. Nadolsky *et al.*, Phys. Rev. **D78**, 013004 (2008), arXiv:0802.0007.
- [39] M. Spira, (1995), arXiv:hep-ph/9510347.
- [40] S. Catani, E. D’Emilio, and L. Trentadue, Phys. Lett. **B211**, 335 (1988).
- [41] D. de Florian and M. Grazzini, Phys. Rev. Lett. **85**, 4678 (2000), arXiv:hep-ph/0008152.
- [42] D. de Florian and M. Grazzini, Nucl. Phys. **B616**, 247 (2001), arXiv:hep-ph/0108273.
- [43] A. Vogt, S. Moch, and J. A. M. Vermaseren, Nucl. Phys. **B691**, 129 (2004), hep-ph/0404111.
- [44] R. P. Kauffman, Phys. Rev. **D45**, 1512 (1992).
- [45] C. P. Yuan, Phys. Lett. **B283**, 395 (1992).
- [46] D. Stump *et al.*, JHEP **10**, 046 (2003), arXiv:hep-ph/0303013.
- [47] J. Pumplin, J. Huston, H. L. Lai, W.-K. Tung, and C. P. Yuan, Phys. Rev. **D80**, 014019 (2009), arXiv:0904.2424.
- [48] CDF - Run II, A. Abulencia *et al.*, Phys. Rev. **D75**, 092006 (2007), arXiv:hep-ex/0701051.
- [49] CDF, T. Aaltonen *et al.*, Phys. Rev. **D78**, 052006 (2008), arXiv:0807.2204.